Supporting Information

Bismuth Iron Molybdenum Oxide Solid Solutions: A Novel and Durable Electrocatalyst for Overall Water Splitting

Sakila Khatun and Poulomi Roy*

Materials Processing & Microsystems Laboratory, CSIR – Central Mechanical Engineering Research Institute (CMERI), Mahatma Gandhi Avenue, Durgapur 713209, West Bengal, India.

Academy of Scientific and Innovative Research (AcSIR), Ghaziabad 201002, Uttar Pradesh, India.

*Email: poulomiroy@yahoo.com, p.roy@cmeri.res.in

Experimental Section

Materials Synthesis

All the chemicals used in the experiments were of analytical grade and were used without any further purification. In a typical procedure, 20 mM bismuth (III) nitrate pentahydrate (Alfa Aesar, ACS, ≥98%) and 10 mM sodium molybdate dihydrate (Sigma-Aldrich, ACS, *≥99%)* were dissolved into 40 ml mixture of water and propionic acid (2:1) under continuous stirring. After 30 min stirring, the mixture was transferred into a teflon-lined autoclave reactor of 50 ml capacity for solvothermal process. The reactor was placed in a hot-air-oven at 180 °C for 16h. After completion of the reaction, the reactor was allowed to cool naturally to room temperature. The precipitation was collected, filtered and washed several times with deionized water, acetone and ethanol, followed by drying at 80 °C in an oven for 8 hr. The resulting sample was then calcined in air at 400 °C for 2 hr to obtain pristine Bi_2MoO_6 with flower-like morphology.

The incorporation of iron was carried out in similar way at 180 °C adding three different mol% of Iron (III) nitrate nonahydrate (Merck, ≥98%) (3 mol%, 6 mol% and 9 mol%) to the total metal precursors. The materials were collected, filtered and washed thoroughly as described earlier. Finally, the materials were calcined at 400 °C in air for 2 hr to obtain three different iron promoted samples. Throughout the manuscript, the samples were abbreviated as BMO for pristine Bi_2MoO_6, BFMO-1 for 3 mol%, BFMO-2 for 6 mol% and BFMO-3 for 9 mol% iron incorporated samples.

Structural Characterization

The X-ray diffraction (XRD) patterns of the materials were recorded using a D2 PHASER (Bruker, Germany) in the 2θ range of 10−80° using Cu K∞ radiation (λ = 1.5418 Å). The morphology of the samples was characterized by field emission scanning electron microscopy (FE-SEM, Carl Zeiss, Germany) at 5 kV, and the compositions of the samples were determined by an energy-dispersive X-ray (EDX) spectrometer associated with FE-SEM. The microstructures of the samples were examined by high-resolution transmission electron microscopy (HR-TEM) on a TECNAI G^2, FEI (Netherland), operating at 200 kV. The TEM specimens were prepared by dispersing powder samples under sonication in pure ethanol (99.999%) to avoid probable oxidation reaction with water and then drop casted on carbon-coated Cu grids followed by drying in vacuum overnight. X-ray photo-electron spectroscopy (XPS) was performed on a SCIENTA, R-3000 Analyzer using a monochromatic Al Kα source (hν = 1,486.6 eV). The typical vacuum in the analysis chamber during the measurements was in the range of 1×10^{-10} Torr. Charge neutralization was used for all measurements using a combination of low-energy Ar^+ ions and electrons. The binding energy scale was charge referenced to the C 1s at 284.6 eV. The Brunauer–Emmett–Teller (BET) measurements were performed by Nitrogen adsorption/ desorption isotherms to investigate the surface characteristics of samples at 77 K using a surface area analyzer (Quantachrome Autosorb IQ3).

Electrochemical Experiments

All electrochemical measurements were conducted in Biologic SP-150 at room temperature using 1 M KOH (pH=13.8) as electrolyte. The working electrodes are composed of samples dropcasted on Ni foam (NF) of 2x1 cm^2 area. Prior to the dropcasting of samples, NFs were treated in 1 M HCl for 10 min under ultra-sonication followed by washing with deionized and ethanol. For dropcasting, the homogeneous sample ink was prepared by dispersing 2 mg sample powder with 100 μl of PVDF solution and 900 μl of water and isopropanol solution with 2:1 ratio under sonication for 20 min. The working electrodes for developed electrocatalysts, i.e, BMO, BFMO-1, BFMO-2, BFMO-3 were prepared by dropcasting 600 μl of sample ink onto the treated 2x1 cm^2 NF with mass loading between 0.8 mg cm^{-2} and 1.0 mg cm^{-2}. For RuO_2 and Pt/C electrode preparation, respective inks were prepared by dispersing 10 mg of commercial RuO_2 powder (Sigma-Aldrich) or 10 wt% Pt/C (Sigma-Aldrich) in 900 μL of isopropanol and water (1:2) and 100 μL of PVDF solution via sonication for 20 min. The treated 2x1 cm^2 NF was soaked in the respective inks followed by drying at 80 °C for 2 h to obtain respective electrodes of mass loading 1 mg/cm^2 for comparative study.

In a three electrode system, linear sweep voltammograms (LSVs) of catalysts were obtained from 0 to 0.8 V in 1 M KOH against saturated Ag/AgCl reference electrodes and

Pt wire as counter electrode at a sweep rate of 0.1 mV s^{-1} for OER and –1 to –1.5 V for HER at sweep rate of 1 mV s^{-1}. The polarization curves were 100% iR corrected in order to avoid the uncompensated resistance. The HER mechanism of samples likely to follow the Volmer-Heyrovsky mechanism as per the stated equation:

$$M + H_2O + e^- \rightarrow M\text{–}H_{ads} + OH^- \qquad \text{(S1)}$$

$$M\text{–}H_{ads} + H_2O + e^- \rightarrow M + H_2 + OH^- \qquad \text{(S2)}$$

The electrochemical impedance spectroscopy (EIS) was conducted in a frequency range 10 kHz to 400 mHz with a perturbing AC potential of magnitude 10 mV at overpotentials that are 300 mV anodic from the onset potential for OER and 280 mV cathodic from the onset potential for HER. Chronoamperometry and chronopotentiometry studies were carried out without iR compensation. The electrochemical surface area (ECSA) of prepared catalyst were studied through the double-layer capacitance (C_{dl}) measurements from the scan-rate-dependent CV plots in the double-layer charging current density built by acquiring in non-Faradaic regions near the oxygen evolution regions and hydrogen evolution regions for OER and HER, respectively. In three-electrode system, the potential scales were converted into a reversible hydrogen electrode (RHE) using the following eq 1:

$$E_{RHE} = E_{Ag/AgCl} + 0.197 + 0.059 \text{ x pH} \qquad \text{(S3)}$$

The overpotential values after iR correction for both OER and HER have been calculated as per the following equations:

$$\eta_{OER} = E_{RHE} – 1.23 \text{ V} – iR \qquad \text{(S4)}$$

$$\eta_{HER} = E_{RHE} – 0 \text{ V} – iR \qquad \text{(S5)}$$

Further, the statistical analysis of iR corrected overpotential values of the electrodes were carried by using standard deviation formula:

$$\sigma = \sqrt{\frac{\sum(x_i - \mu)^2}{N}} \qquad \text{(S6)}$$

Where, σ = Standard deviation; $x_i =$ Values of the populations, N= Size of the population and μ = Population mean.

The overall water splitting analyses were carried out in a two-electrode system using the catalysts as anode and cathode in 1M KOH electrolyte. All the experiments were carried out in room light. However, no light excitation was observed switching room light – dark – room light in chronoamperometry study or comparing LSV plots under dark or room light.

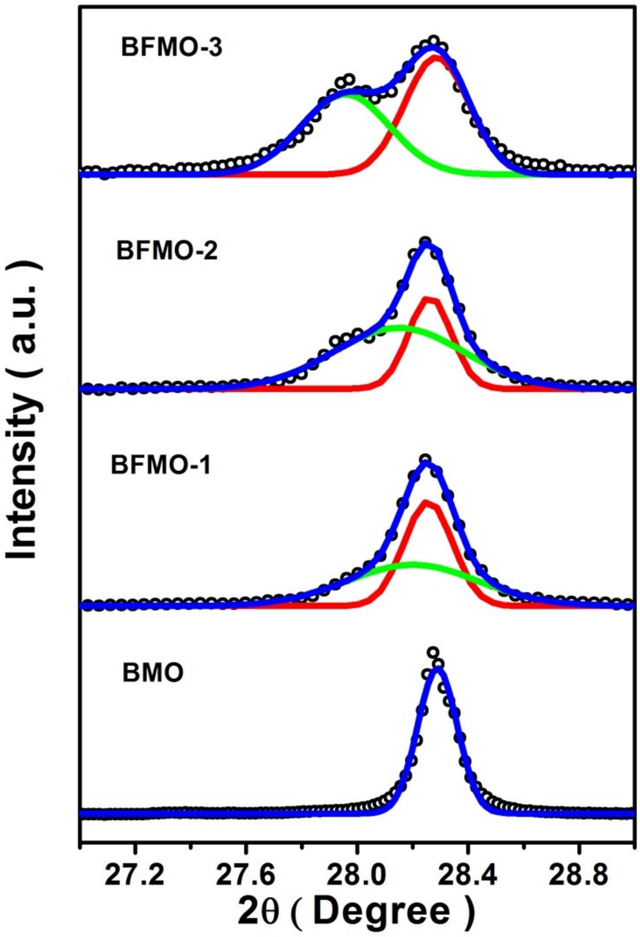

Figure S1: Magnified view of XRD pattern with deconvoluted peaks of (131) for Bi_2MoO_6 (red) and (221) for $Bi_3(FeO_4)(MoO_4)_2$ (green).

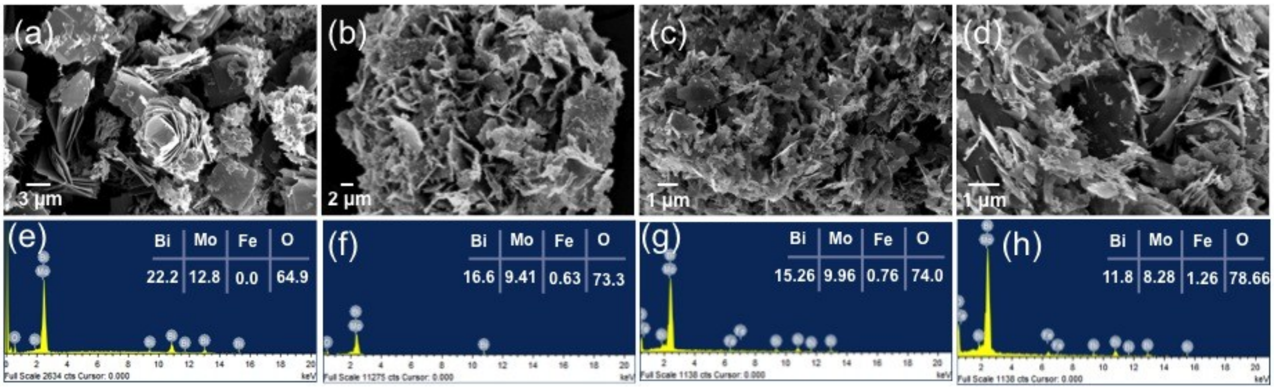

(e)

Bi	Mo	Fe	O
22.2	12.8	0.0	64.9

(f)

Bi	Mo	Fe	O
16.6	9.41	0.63	73.3

(g)

Bi	Mo	Fe	O
15.26	9.96	0.76	74.0

(h)

Bi	Mo	Fe	O
11.8	8.28	1.26	78.66

Figure S2: (a-d) FESEM and (e-h) EDX analyses of BMO (a, e); BFMO-1 (b, f); BFMO-2 (c, g) and BFMO-3 (d, h).

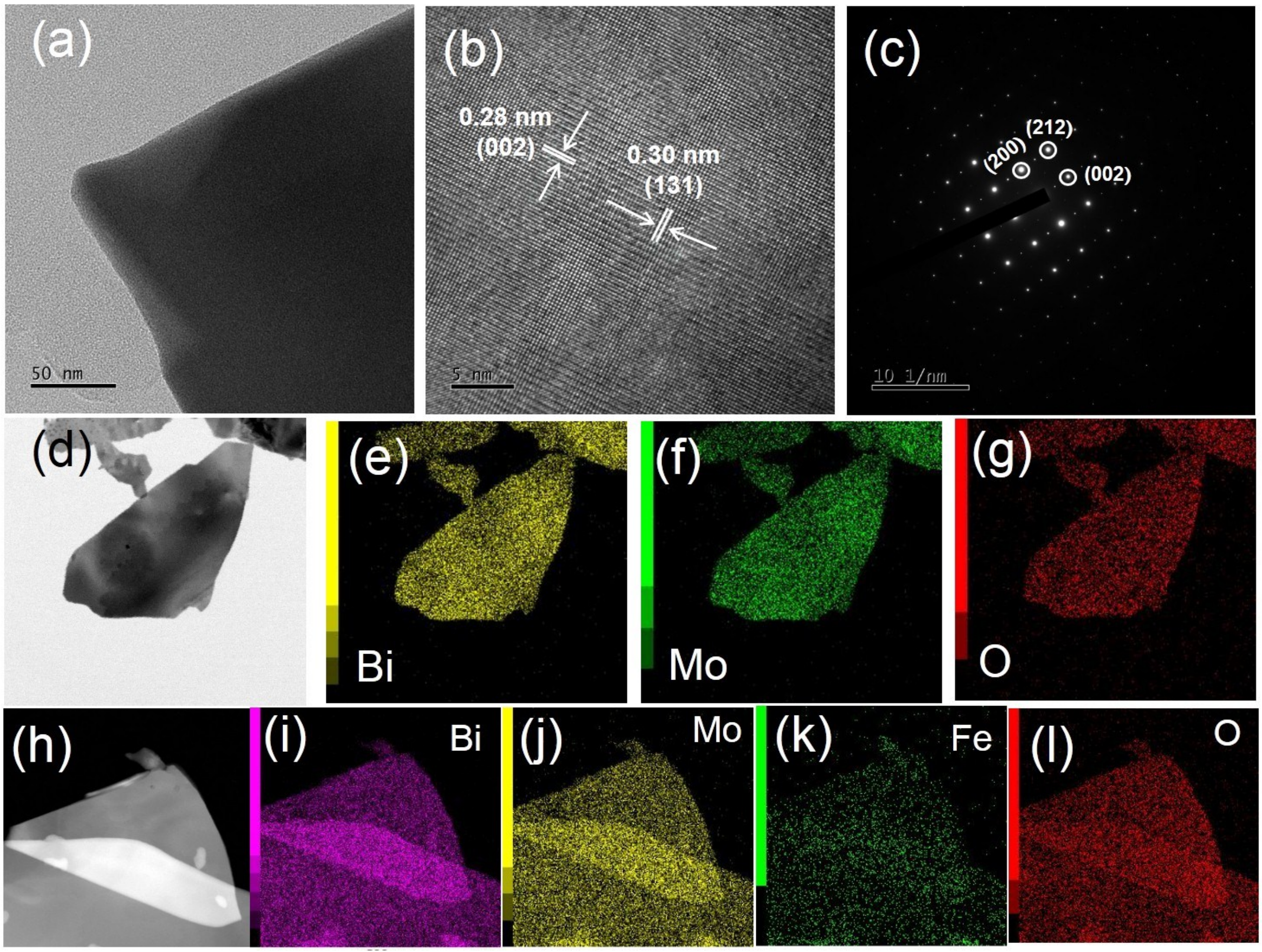

Figure S3: (a) TEM and (b) HRTEM images of BMO and (c) corresponding SAED pattern. (d-l) STEM elemental mapping for Bi, Mo and O for BMO (d-g) and Bi, Mo, Fe and O for BFMO-1 (h-l) showing homogeneous distribution of elements through out nanoplates.

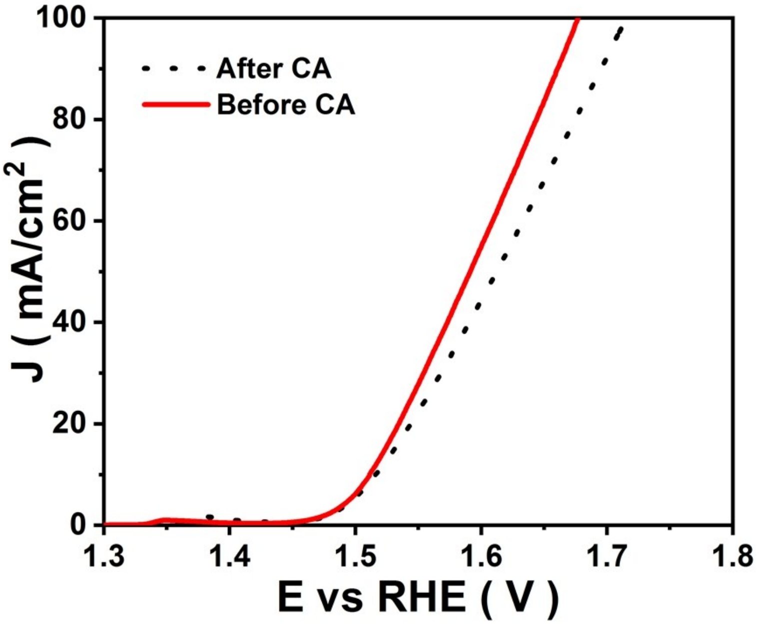

Figure S4: LSV plot for OER of BFMO-2 before and after chronoamperometry (CA) test.

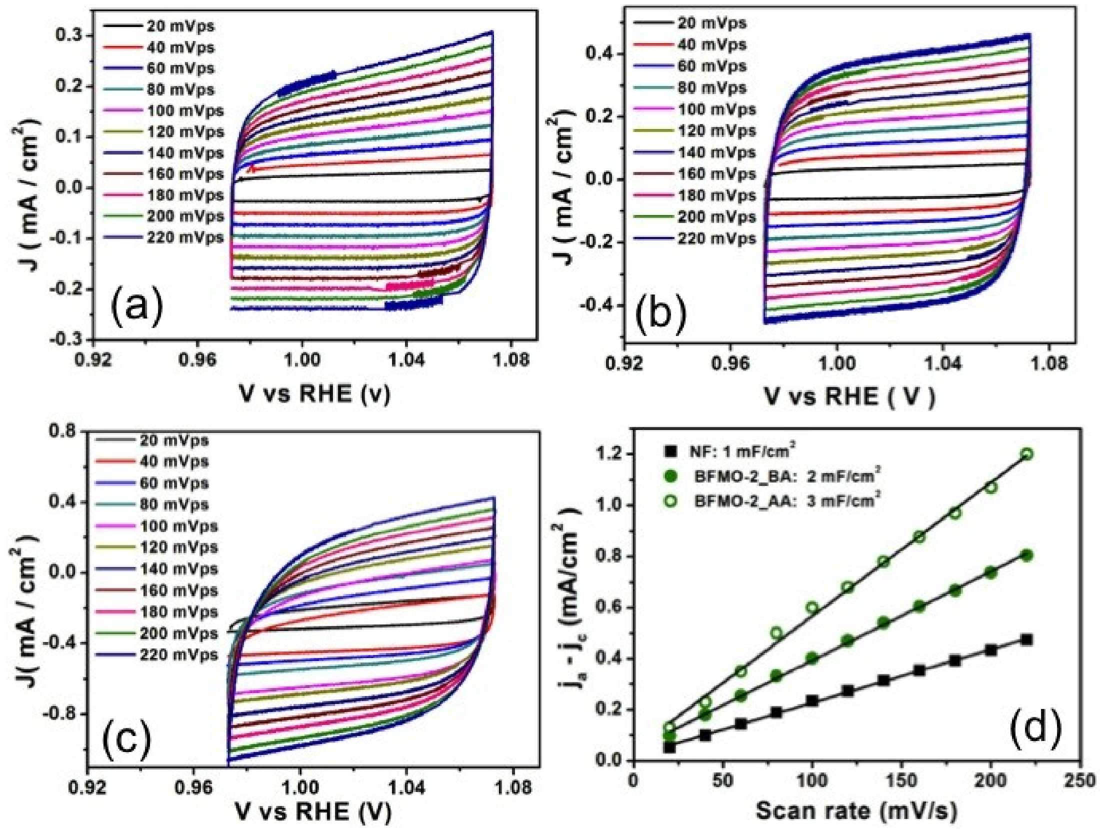

Figure S5: (a-c) Cyclic voltammograms recorded for (a) NF, (b) BFMO-2 before CA, (c) BFMO-2 after CA electrodes at various scan rates in the non-Faradaic region; (d) Plot of current density differences between anodic and cathodic to determine the double layer (C_{dl}) capacitance values of OER.

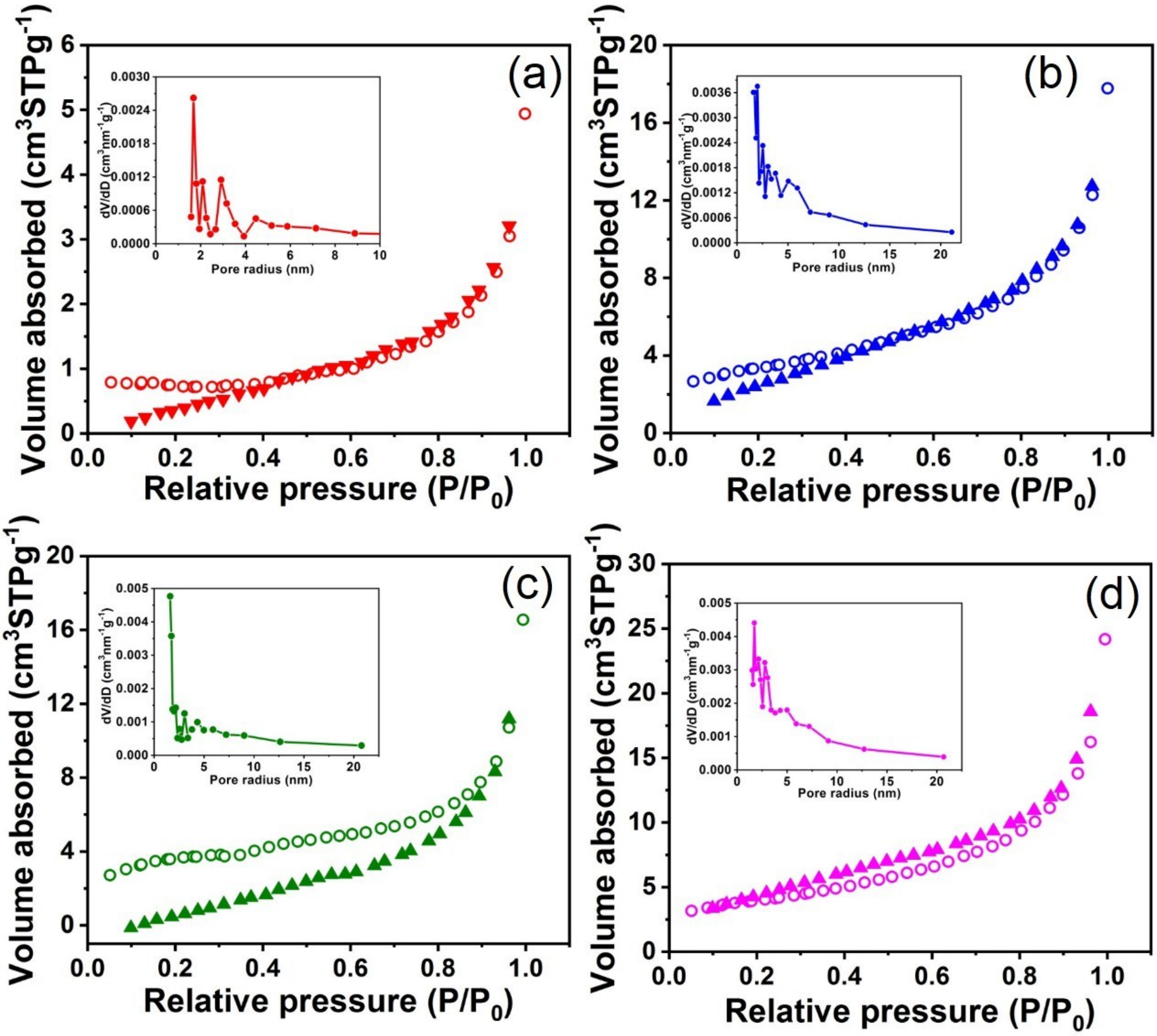

Figure S6: N_2 adsorption-desorption isotherm with pore size distribution curves (a) BMO (b) BFMO-1 (c) BFMO-2 (d) BFMO-3 samples.

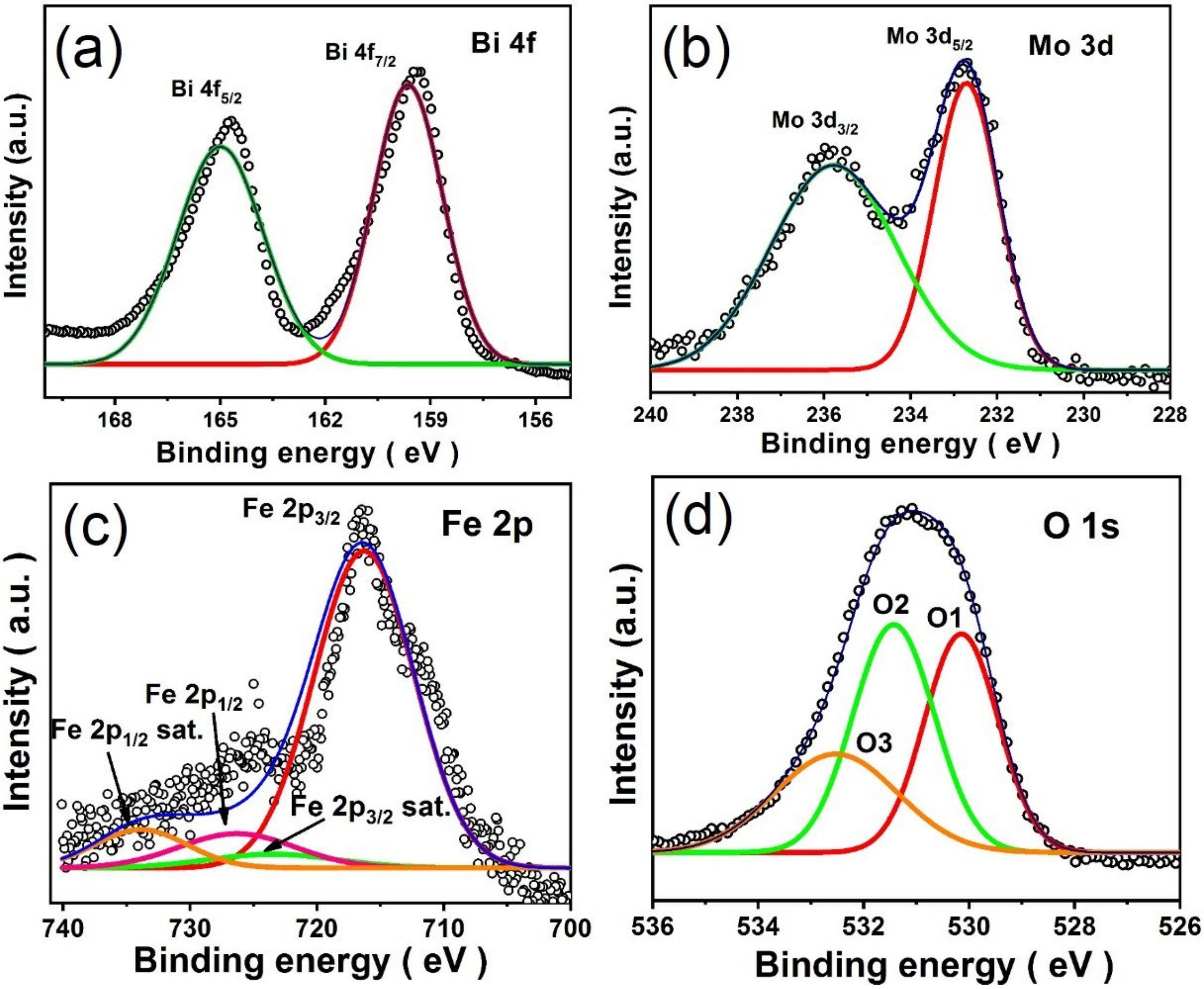

Figure S7: High-resolution spectra of Bi 4f (a), Mo 3d (b), Fe 2p (c) and O 1s (d) for BFMO-2 after chronoamperometric analysis for OER.

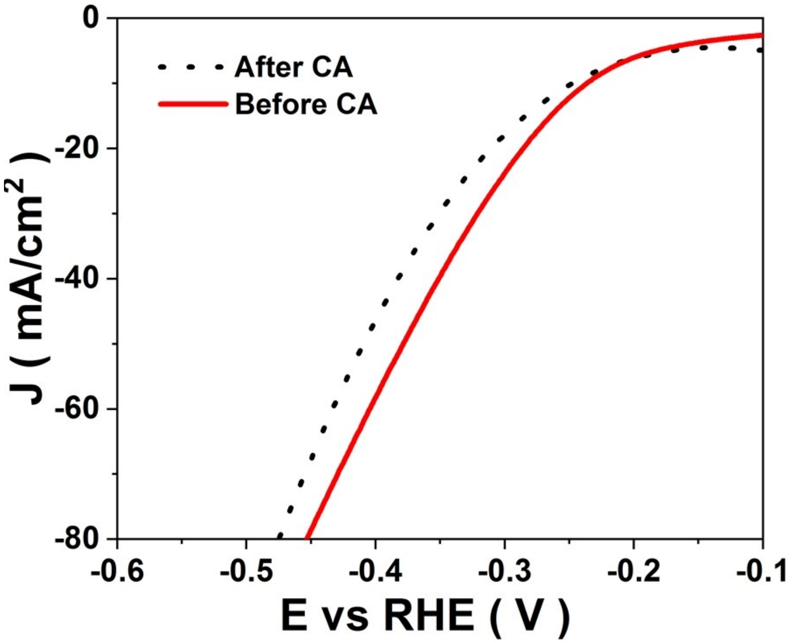

Figure S8: LSV plot for HER of BFMO-2 before and after chronoamperometry (CA) test.

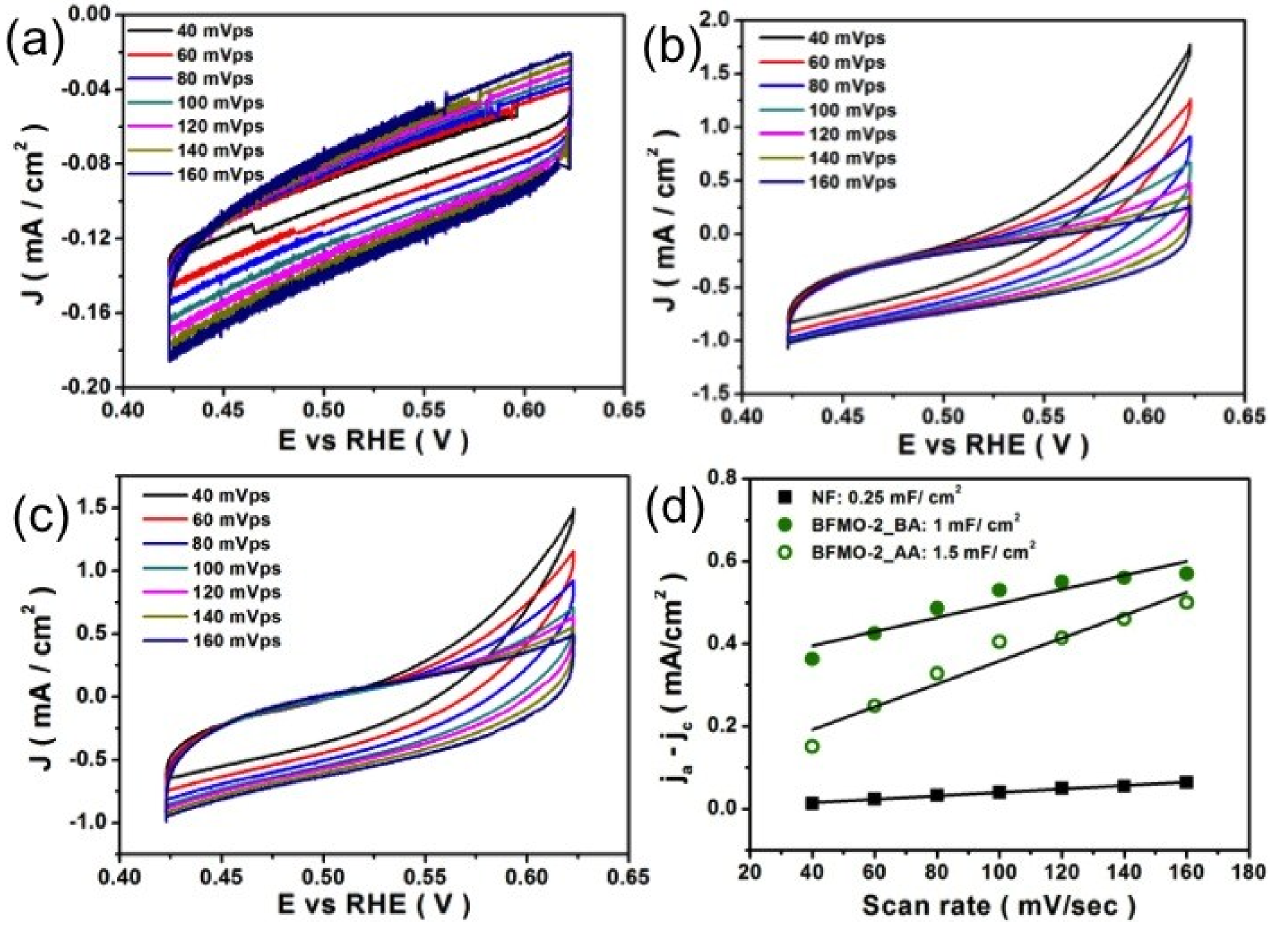

Figure S9: Cyclic voltammograms recorded (a) NF (b) BFMO-2 before CA (c) BFMO-2 after CA electrodes at various scan rates to determine the double layer (C_{dl}) capacitance of HER (d) Plot of current density differences between anodic and cathodic at different scan rates for determining C_{dl} values of BFMO-2 before and after activation for HER.

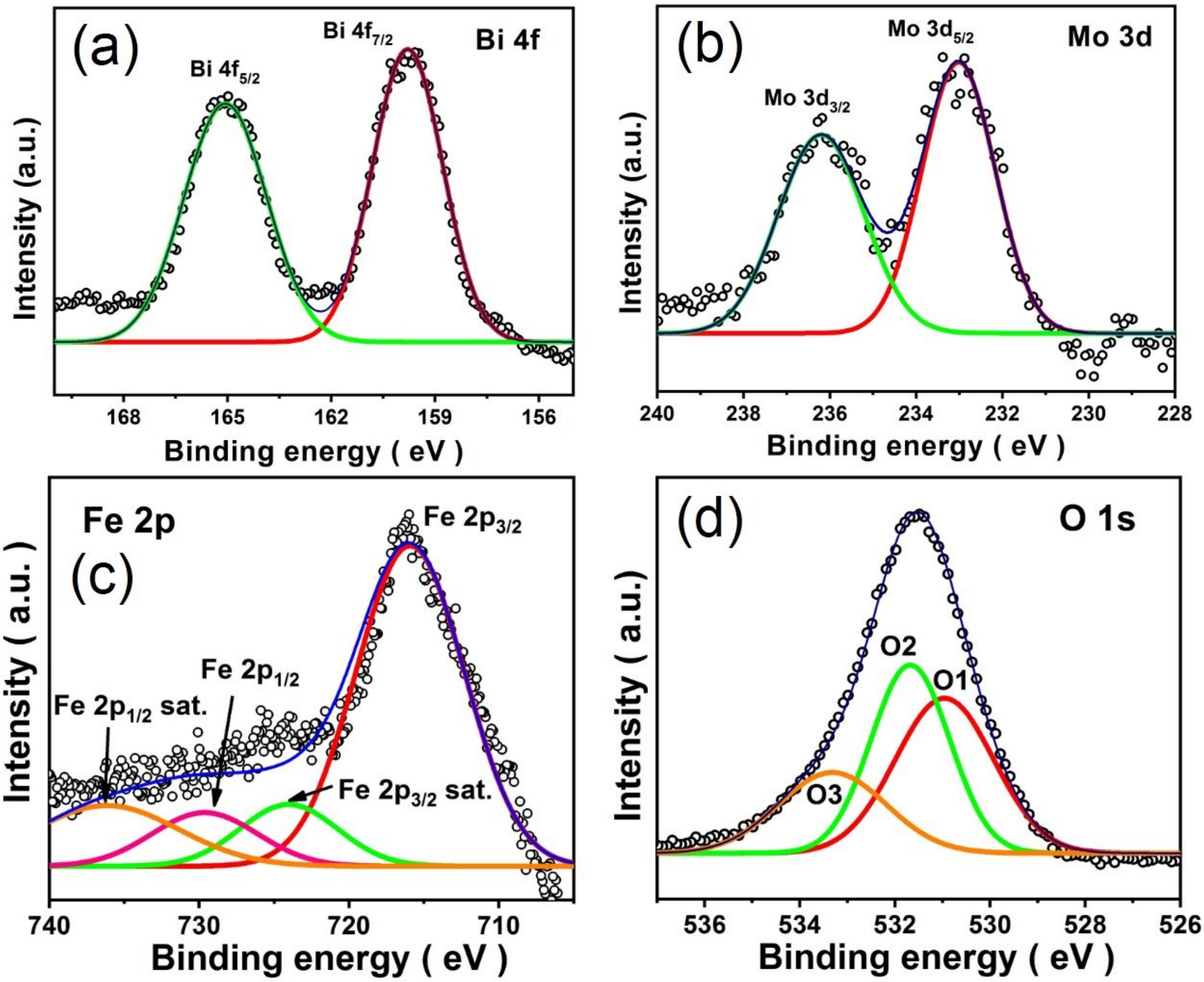

Figure S10: High-resolution spectra of Bi 4f (a), Mo 3d (b), Fe 2p (c) and O 1s (d) for BFMO-2 after chronoamperometric analysis for HER.

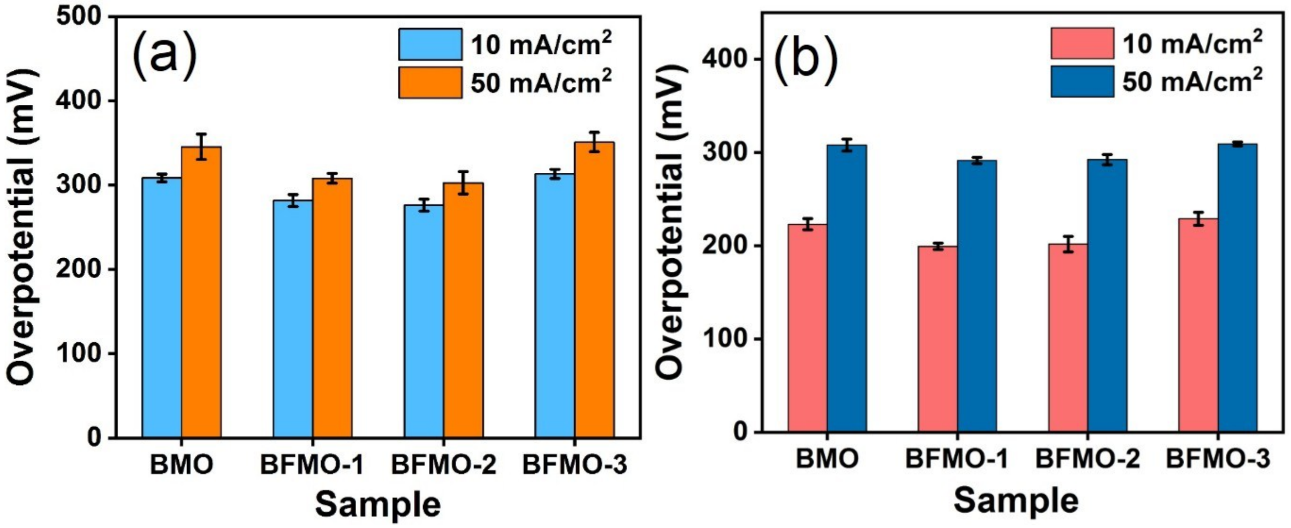

Figure S11: Statistical analysis of overpotential values obtained at 10 mA cm^{-2} and 50 mA cm^{-2} current densities after iR correction for OER (a) and HER (b), showing reproducibility of the electrocatalytic performances.

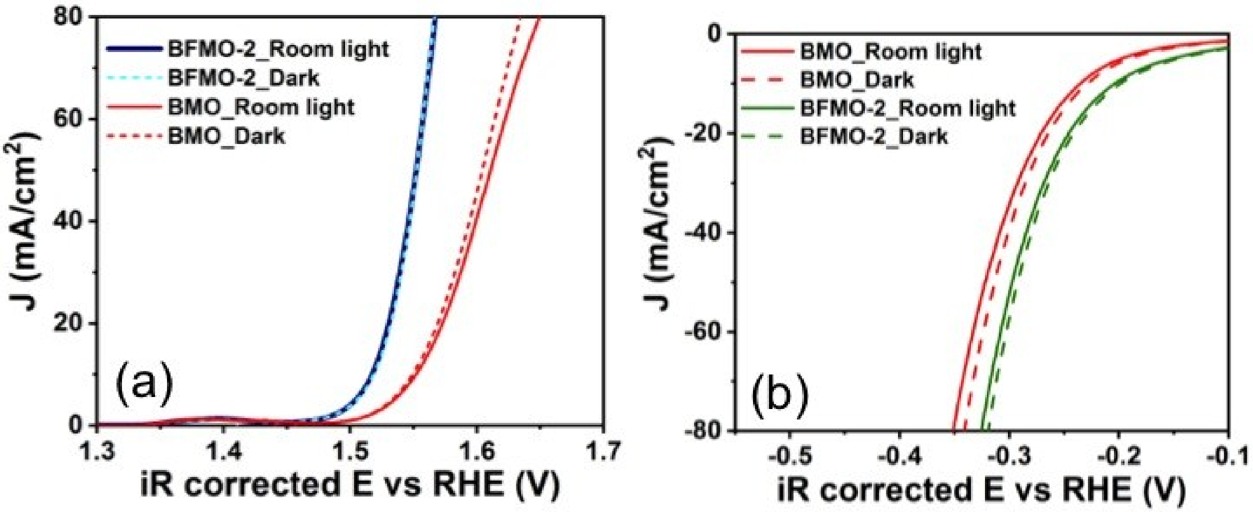

Figure S12: LSV plots of BFMO-2 and BMO for OER (a) and HER (b) performed in room light and under dark show no influence of light, indicating electrocatalytic performance only.

Table S1: Electrical resistivity values of samples derived from EIS analysis for OER and HER mechanisms.

Samples	OER		HER	
	R_s (ohm)	R_{ct} (ohm)	R_s (ohm)	R_{ct} (ohm)
NF	1.06	4.23	1.44	5.45
RuO2	1.50	2.67	--	--
10wt% Pt/C	--	--	1.30	1.60
BMO	1.55	0.43	1.75	2.88
BFMO-1	1.60	0.42	1.67	3.27
BFMO-2	1.20	0.28	1.62	2.26
BFMO-3	1.60	0.70	1.3	4.10

Table 2: Comparative table of some bifunctional catalysts and their performances in overall water splitting in alkaline medium.

Electrocatalytic system	**Medium**	**Overall potential @10 mA cm^{-2}**	**Durability**	**References**
$NiCo_2O_4$/Ni || $NiCo_2O_4$/Ni	1M NaOH	1.65 V	36 h	S1
Ni_3Se_4/Ni || Ni_3Se_4/Ni	3M KOH	1.66 V (@50 mA cm^{-2})	9 h	S2
Ni_2P/Ni || Ni_2P/Ni	1M KOH	1.6 V	12 h	S3
NiFeOF || NiFeOF	1M KOH	1.55 V	3 h	S4
$P_{8.6}$-Co_3O_4/NF || $P_{8.6}$-Co_3O_4/NF	1M KOH	1.63 V	25 h	S5
$NiCo_2O_4$/Ti || $Ni_{0.33}Co_{0.67}S_2$/Ti	1M KOH	1.65 V (@5 mA cm^{-2})	20 h	S6
CuCoO/NF || CuCoO/NF	1M KOH	1.61 V	72 h	S7
$NiCo_2S_4$/NF || $NiCo_2S_4$/NF	1M KOH	1.63 V	50 h	S8
CoS_2/CC || CoS_2/CC	1M KOH	1.67 V	20 h	S9
CoMoSx/NF || CoMoSx/NF	1M KOH	1.8 V	25 h	S10
$SrNb_{0.1}Co_{0.7}Fe_{0.2}O_{3-\delta}$/NF || $SrNb_{0.1}Co_{0.7}Fe_{0.2}O_{3-\delta}$/NF	1 M KOH	1.68 V	30 h	S11
CoNi-OOH|Ti || CoNi-OOH|Ti	1 M KOH	1.76 V	60 h	S12
$Bi_xFe_{x-2}(MoO_6)_{x-1}$/NF || $Bi_xFe_{x-2}(MoO_6)_{x-1}$/NF	1 M KOH	1.67 V	100 h	This work

References

S1. X. Gao, H. Zhang, Q. Li, X. Yu, Z. Hong, X. Zhang, C. Liang, Z. Lin, *Angew. Chem. Int. Ed.* **2016,** *55*, 6290-6294.

S2. S. Anantharaj, J. Kennedy, S. Kundu, *ACS Appl. Mater. Interfaces* **2017,** *9*, 8714-8728.

S3. P. W. Menezes, A. Indra, C. Das, C. Walter, C. Göbel, V. Gutkin, D. Schmeiβer, M. Driess, *ACS Catal.* **2017,** *7*, 103-109.

S4. K. Liang, L. Guo, K. Marcus, S.-F. Zhang, Z. Yang, D. E. Perea, L. Zhou, Y. Du, Y. Yang, *ACS Catal.* **2017,** *7*, 8406-8412.

S5 Z. Wang, H. Liu, R. Ge, X. Ren, J. Ren, D. Yang, L. Zhang, X. Sun, *ACS Catal*. **2018,** *8, 3*, 2236-2241.

S6. Z. Peng, D. Jia, A. M. A. Enizi, A. A. Elzatahry, G. Zheng, *Adv. Energy Mater.* **2015**, *5*, 1402031.

S7. M. Kuang, P. Han, Q. Wang, J. Li, G. Zheng, *Adv. Funct. Mater*. **2016**, *26*, 8555–8561.

S8. A. Sivanantham, P. Ganesan, S. Shanmugam, *Adv. Funct. Mater.* **2016**, *26*, 4661–4672.

S9. C. Guan, X. Liu, A. M. Elshahawy, H. Zhang, H. Wu, S. J. Pennycook, J. Wang, *Nanoscale Horiz.*, **2017**, *2*, 342-348.

S10. S. Shit, W. Jang, S. Bolar, N. C. Murmu, H. Koo, T. Kuila, *ACS Appl. Mater. Interfaces* **2019,** *11*, 21634-21644.

S11. Y. Zhu, W. Zhou, Y. Zhong, Y. Bu, X. Chen, Q. Zhong, M. Liu, Z. Shao, *Adv. Energy Mater*. **2017**, *7*, 1602122.

S12. C. Yu, J. Lu, L. Luo, F. Xu, P. K. Shen, P. Tsiakaras, S. Yin, *Electrochim. Acta*. **2019**, *301*, 449-457.